

Anatomy of an extreme event: What can we infer about the history of a heavy-tailed random walk?

Wesley W. Erickson  and Daniel A. Steck 

*Oregon Center for Optical, Molecular, and Quantum Science and Department of Physics,
1274 University of Oregon, Eugene, Oregon 97403-1274, USA*

Extreme events are by nature rare and difficult to predict, yet are often much more important than frequent, typical events. An interesting counterpoint to the *prediction* of such events is their *retrodiction*—given a process in an outlier state, how did the events leading up to this endpoint unfold? In particular, was there only a single, massive event, or was the history a composite of multiple, smaller but still significant events? To investigate this problem we take heavy-tailed stochastic processes (specifically, the symmetric, α -stable Lévy processes) as prototypical random walks. A natural and useful characteristic scale arises from the analysis of processes conditioned to arrive in a particular final state (Lévy bridges). For final displacements longer than this scale, the scenario of a single, long jump is most likely, even though it corresponds to a rare, extreme event. On the other hand, for small final displacements, histories involving extreme events tend to be suppressed. To further illustrate the utility of this analysis, we show how it provides an intuitive framework for understanding three problems related to boundary crossings of heavy-tailed processes. These examples illustrate how intuition fails to carry over from diffusive processes, even very close to the Gaussian limit. One example yields a computationally and conceptually useful representation of Lévy bridges that illustrates how conditioning impacts the extreme-event content of a random walk. The other examples involve the conditioned boundary-crossing problem and the ordinary first-escape problem; we discuss the observability of the latter example in experiments with laser-cooled atoms.

PACS numbers: 05.40.Fb, 02.50.Ey, 02.50.-r

I. INTRODUCTION

Extreme events affect us in many ways, from geological and meteorological phenomena to market crashes and epidemics, and both science and society have been increasingly appreciating the need to understand and plan for such events [1, 2]. Gaussian stochastic models fail to predict extreme events, which are commonly associated with probability distributions with “heavy” power-law tails. Lévy processes (specifically, stable Lévy processes [3–5]) in particular are important prototypes for heavy-tailed random processes exhibiting large jumps or “Lévy flights” (Fig. 1), as they are universal for random walks generated by heavy-tailed distributions, in the same sense that Gaussian processes are universal for finite-variance steps. Lévy processes play an important role in understanding a wide range of phenomena [6, 7], including ecology [8], finance [3], fluid flows [9], chaotic transport [10], stochastic searches [11, 12], and particularly in laser-cooled atoms [13–20]. The stable processes also produce strikingly counterintuitive behavior; for example, intriguing work has shown that the image method fails to predict their first-passage times [21–24].

Of general importance in probability and statistics is the question of inference, which in stochastic processes is embodied by conditioned evolution. The Brownian bridge—a continuous-time Gaussian stochastic process specified to arrive at some final location (state)—is a well known and widely used examples of a conditioned process. The properties and statistics of Brownian bridges have been thoroughly studied [25]; they are pro-

ductively applied in diverse areas, occurring in financial mathematics [26, 27], models of animal movements [28], Monte Carlo methods in quantum mechanics [29, 30], random interfaces and potentials [31–33], and extreme-value statistics [34]. Because Lévy-type statistics arise in a similarly diverse range of applications, and are also a cornerstone of extreme-event science, clearly a detailed study of similarly conditioned, heavy-tailed processes is needed. (An analogous generalization is to fractional Brownian bridges [35], which have been applied to the study of biological autoluminescence [36].) Work on such Lévy bridges is at a nascent stage, however: they have been formalized conceptually and applied to finance and insurance [37, 38], and a few functionals of Lévy bridges have been characterized [39–41].

This paper explores the dynamics of continuous-time Lévy processes $x(t)$ conditioned to arrive at the final state $L = x(T)$. A key question that we address is: Was this arrival a result of a single, large event, or a composite of multiple, smaller events? From the typical behavior of heavy-tailed processes, where rare but large events dominate the evolution, one may expect that when arriving at an extreme state, only a single extreme event is responsible, simply due to their rarity. However, a proper accounting of the responsible events is only possible by analyzing the conditional probabilities for the state at intermediate times. The structure of conditional probability densities for intermediate times $t \in (0, T)$ makes a transition from unimodal to bimodal as the arrival point L varies, leading to interesting and counterintuitive effects, particularly in rare but important cases

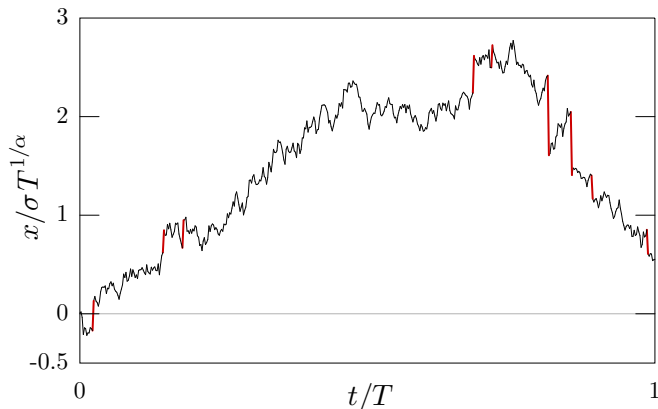


FIG. 1. Sample path of an unconditioned α -stable Lévy process, $\alpha = 1.9$. Simulated path has time steps $\Delta t = T/500$ with increments $\Delta x > L_b(\Delta t/T)^{1/\alpha}$ emphasized (bold/red).

where an extreme jump occurred. Above the bimodal transition, the typical conditioned history contains only a single large event, while below the transition the tendency is towards a composite of smaller events. This analysis provides insight into first-passage problems for stable processes, highlighting dramatic qualitative differences between Gaussian and heavy-tailed processes, even when the latter are “close to” Gaussian. This work also provides a more precise, mathematical basis for the intuition that random variations that occur in between rare, extreme events tend to seem Gaussian, so much so that there is a strong temptation to ignore extreme events in mathematical models, with sometimes devastating consequences [42].

A closely related existing result is the “big-jump principle” [43], which observes under fairly general conditions that for a sum of random variables, in the limit of a large summed value, the distribution of the sum agrees with the distribution of the maximum of the variables. The implication is again that extreme events are dominated by a single largest jump, rather than many small displacements. This holds true even in the case of stretched-exponential processes, with sub-power-law tails [44]. Another closely related concept is that of “condensation” in probability space, which is analogous to the condensation phase in stochastic mass transport where a macroscopically large mass forms at a single site on a lattice [45]. In a stochastic process, the analogous phenomenon is the emergence of one or more jumps responsible for a macroscopic fraction of the total displacement after many steps. Condensation occurs in heavy-tailed processes, but can also occur even in light-tailed processes in the presence of multiple constraints (e.g., conditioning on the values of both the total sum and the sum of squared steps) [46, 47]. In another example, a double transition to the condensed state occurs in the run-and-tumble particle [48]. Our results augment this prior work by providing a length scale defining the crossover to the large-jump regime, which is

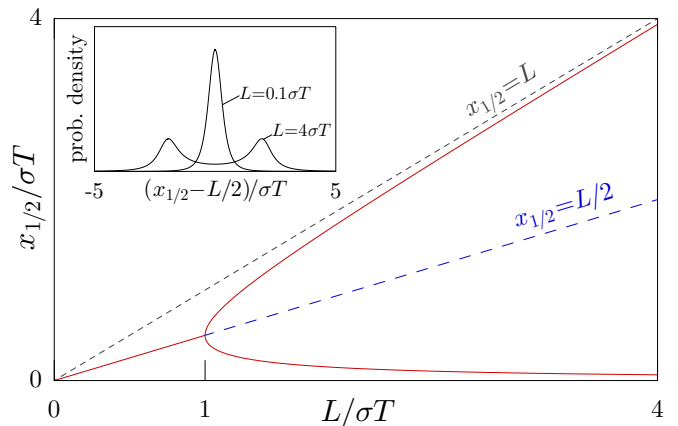


FIG. 2. Bifurcation diagram showing maxima (solid, red) and minima (dashed, blue) of the conditioned density (1) for $\alpha = 1$. Inset: conditioned density before and after the bifurcation.

based on the analysis of conditioned probabilities.

II. DEFINITIONS

The continuous-time α -stable Lévy processes are specified in terms of the characteristic function $\langle e^{ikx(t)} \rangle = e^{-t\sigma^\alpha |k|^\alpha}$ at time t , provided $x(0) = 0$ [5]; the Fourier transform yields the probability density $f_\alpha(x; t)$ for $x(t)$, thus being “stable” under iterated convolutions. For simplicity we will only consider symmetric stable processes. Also, σ is a width-scaling parameter, and $\alpha \in (0, 2]$ characterizes the long tails of the densities. The case $\alpha = 2$ is Gaussian, while $\alpha < 2$ densities have heavy, power-law tails scaling as $|x|^{-(1+\alpha)}$. The variance diverges for $\alpha < 2$ and the mean absolute deviation diverges for $\alpha \leq 1$. The power-law tails are responsible for jump discontinuities in the stochastic evolution that are absent in the Gaussian case. To be precise about terminology, we will refer to these jump discontinuities as “jumps,” while instead using “steps” or “displacements” to refer to the change in state over a finite time interval.

III. BIFURCATION LENGTH

A. Lévy bridges

In a Lévy bridge, the arrival point is specified as $x(T) = L$ for some arrival time $T > 0$. Then the intermediate position $x_{1/2} := x(T/2)$ has the conditional density (“midpoint density”)

$$f_\alpha(x_{1/2}; T/2 | x = L; T) = \frac{f_\alpha(x_{1/2}; T/2) f_\alpha(L - x_{1/2}; T/2)}{f_\alpha(L; T)} \quad (1)$$

in terms of the unconditioned density $f_\alpha(x; t)$. Once $x(T/2)$ is sampled, the bridge is effectively bisected into

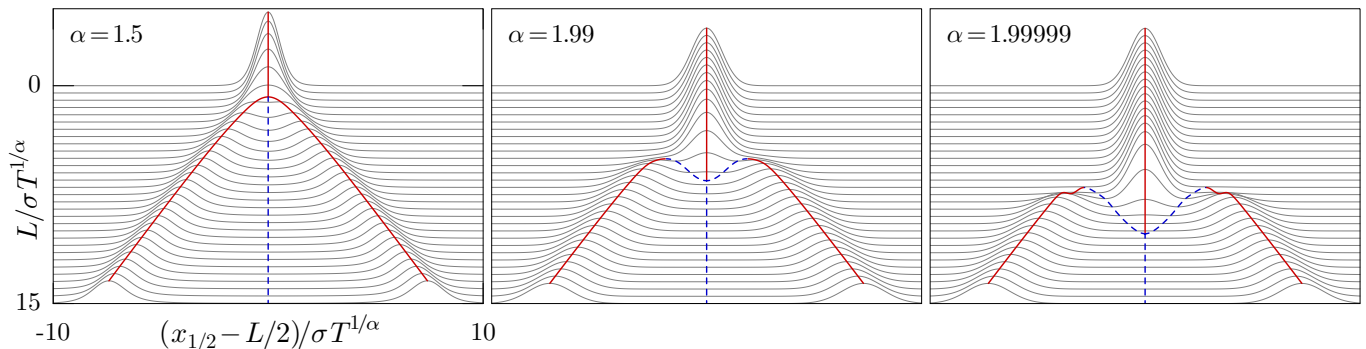


FIG. 3. Variation of the midstep density (1) with Lévy index α and arrival point L . Curves highlighting maxima (solid, red) and minima (dashed, blue) are superimposed.

two bridges, and the midpoint-sampling process may be iterated to sample the Lévy bridge to any desired time resolution. For $\alpha = 2$ the midpoint density retains the same Gaussian form as the unconditioned density, but the conditioned and unconditioned forms differ for any $\alpha < 2$.

The Cauchy ($\alpha = 1$) case is a good example of what happens for $\alpha < 2$. For $L < \sigma T$, this distribution has a single peak at $x_{1/2} = L/2$, which has a seemingly intuitive interpretation: if a particle travels from $x = 0$ to L in time T , the most probable intermediate position at $T/2$ is $L/2$. However, this intuition breaks down at the special arrival point $L_b = \sigma T$, beyond which the midpoint density becomes bimodal, and the single maximum bifurcates into a pair at $x_{1/2} = [L \pm (L^2 - \sigma^2 T^2)^{1/2}]/2$ (Fig. 2). For $L \gg L_b$ the peaks are well separated, with maxima approaching asymptotes $x_{1/2} \sim 0, L$. In this case, the interpretation of the midpoint changes: the large final displacement L tends to break down into one large step of order L and one small step, rather than two steps roughly equal to $L/2$. A bridge with sufficiently large overall transition length L will tend to maintain this as a single jump discontinuity.

Similar structural changes in the midpoint density occur for all $\alpha < 2$. Figure 3 shows typical possibilities of how the bifurcation occurs as L increases. For $\alpha = 1.5$ there is a pitchfork bifurcation [49], as in the Cauchy case, where two maxima and a minimum are created from a single maximum. However, closer to the Gaussian limit ($\alpha = 1.99$ and $\alpha = 1.99999$), the structure is more complicated: first, a pair of side peaks is born via tangent bifurcations; second, the side peaks grow to match the central peak in height; and third, a central minimum forms in a reverse-pitchfork bifurcation. For any α the end results are the same: a unimodal density transforms into a bimodal density with well separated peaks.

B. Variation with α

An obvious characterization of the bifurcation length L_b is the value of L for which the curvature of the mid-

point density (1) at $x_{1/2} = L/2$ changes sign (Fig. 4). However, for α above a critical value α_c , as we have seen, the midpoint density does not exhibit a simple bifurcation to a bimodal density; rather, there are three distinct transitions. [The critical value $\alpha_c \approx 1.7999233$ occurs when the fourth derivative of the midpoint density (1) vanishes at $x_{1/2} = L/2$ (in addition to the vanishing of the second derivative, which already defines L_b).] All three bifurcation lengths are shown in Fig. 4 for $\alpha > \alpha_c$. They all usefully characterize the structural changes of the distribution, though in practice the particular choice of L_b is not too important—as we will see, the transition between “short” and “long” displacements is not sharp. (We use the curvature-change criterion except where noted.)

Figure 4 also shows the transition away from power-law tails in the limit $\alpha \rightarrow 2$. The bifurcation length diverges in this limit, so that for the Gaussian ($\alpha = 2$) case, any final step L is a “short step.” The nature of this divergence may be analyzed using the asymptotic density $f_\alpha(x; t = 1) \sim f_2(x; 1) + \delta|x|^{\delta-3}$, valid for large $|x|$ and small $\delta := 2 - \alpha$ [50]. One can show that L_b (defined by the curvature-sign-change criterion) diverges as $L_b \sim [-4\sigma^2 T \log(\pi\delta^2/2)]^{1/2}$. Numerically, L_b seems to diverge similarly according to the other criteria as well. Thus, even very close to the Gaussian limit $\alpha = 2$, L_b remains relatively small (cf. Fig. 3, third panel).

C. Conditioned sampling

As noted above, when sampling the intermediate state of a Lévy bridge for $L > L_b$, a jump of order L likely persists. Upon further recursive subsampling of the bridge’s intermediate states, this behavior locks in: L_b is effectively smaller when sampling sub-bridges on progressively smaller time intervals, so that the substep length L tends to exceed L_b by an ever increasing margin, making it progressively less likely to be split into smaller jumps. Figure 5 illustrates this: for $L = 1.5L_b$ there is typically a single long step that persists to high temporal resolution. By contrast, for $L = 0.5L_b$, the overall displacement has decomposed into many small steps, with

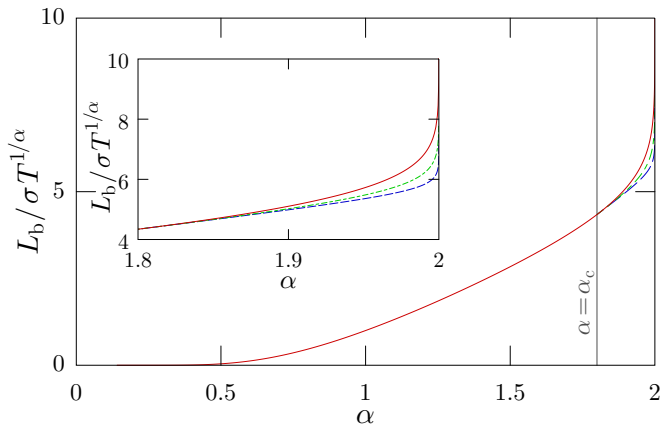


FIG. 4. Variation of boundaries between “small” and “large” steps with α . Curves indicate bifurcation lengths L_b for which the center of the midstep density has vanishing curvature (red, solid), the half-step distribution develops side peaks (blue, dashed), and side peaks are equal in height to the center peak (green, dot-dashed). Inset: magnified view for $\alpha > \alpha_c$.

an appearance resembling Brownian motion. The intermediate case $L = L_b$ exhibits both behaviors.

This behavior under conditioned subsampling shows that the bifurcation length L_b yields an innate notion of large steps of an α -stable process. Specifically, an observed final displacement $|x(T)| \gg L_b$ most likely corresponds to a single, similarly large jump discontinuity, even if the detailed evolution up to the final time T is not known. Meanwhile, a smaller final displacement $|x(T)| \lesssim L_b$ is more likely to be a composite event comprising multiple smaller jumps. This latter conclusion can be understood from the tails of the conditioned density (1), which scale as $|x|^{-2(1+\alpha)}$, which are relatively short compared to the $|x|^{-(1+\alpha)}$ tails of the step density $f_\alpha(x;t)$. This is a powerful qualitative inference based only on the endpoints of the process; it is useful in problems of interpolation of a stochastic process between observations (e.g., animal movement [28] and kriging [51]), if the underlying process is heavy-tailed. Additionally, this provides a means for inferring whether a rare, significant event occurred between observations. Such criteria are important for the analysis of statistical extremes [2] and for specific problems like detecting market crashes [52].

A salient feature of stable Lévy processes is scale-invariance. So how is it possible to have an intrinsic scale L_b ? Scale invariance is best seen in the Lévy–Khintchine representation [3–5], where symmetric stable processes have pure power-law jump-rate densities $\sin(\pi\alpha/2)\Gamma(1+\alpha)\sigma^\alpha/(\pi|\Delta x|^{1+\alpha})$. In some sense, then, any scale based solely on the step distribution (width at half maximum, etc.) is inherently nonsensical. However, conditioning introduces a timescale T , which induces a length scale—one that can only be understood through the variable structure of the conditioned density (1). Importantly, this scale differs from the well known length

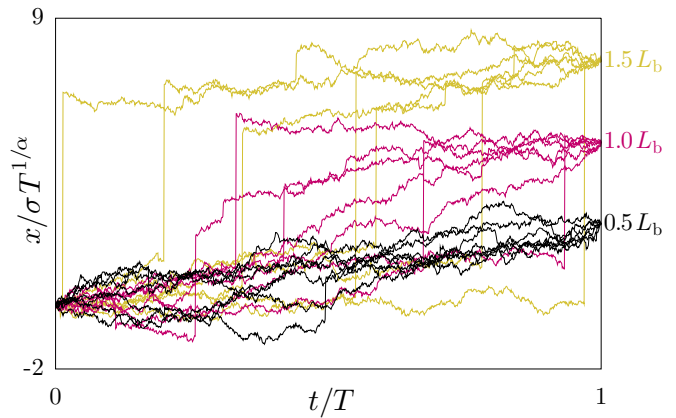


FIG. 5. Typical sample paths of Lévy bridges for $\alpha = 1.9$, illustrating the qualitative transition with L . Each path was generated through 10 recursive subsamplings from the midstep distribution (1).

scale $\sigma T^{1/\alpha}$ [43, 44]. This distinction defines an intuitive notion of “long” displacements that captures how, visually and intuitively, the large-scale structure of stable Lévy processes seem similar to Gaussian processes punctuated by discrete jump discontinuities (Fig. 1). Mathematically, this similarity is not obvious: Stable Lévy processes with $\alpha < 2$ have a dense set of discontinuities, whereas Gaussian processes are continuous (almost surely).

IV. APPLICATIONS

A. Stretched Lévy bridges

In the Gaussian case, one important representation of the Brownian bridge is [53]

$$W(t) = B(t) + \frac{t}{T}[W(T) - B(T)], \quad (2)$$

where $W(t)$ is a Wiener process (unconditioned Lévy process with $\alpha = 2$, $\sigma = 1/\sqrt{2}$), and $B(t)$ is a Brownian bridge [Wiener process conditioned to have a fixed arrival $B(T)$]. Intuitively, in the “standard bridge” case $B(T) = 0$, the second term is the ballistic trajectory from 0 to $W(T)$, while $B(t)$ comprises the random fluctuations. This representation, when interpreted as an expression for $B(t)$ in terms of $W(t)$ and the ballistic motion, provides a simple way to simulate Brownian bridges using any Wiener-process algorithm. Naively, it seems like this representation should be valid for $\alpha < 2$ stable processes: Dividing the evolution into time steps Δt , the increments of the stable process and bridge are of order $\Delta t^{1/\alpha}$, while the ballistic correction is of order Δt . The ballistic component is thus of order $\Delta t^{1-1/\alpha}$ relative to the Lévy-process steps, and thus should be negligible as $\Delta t \rightarrow 0$ provided $\alpha > 1$. In the Gaussian case this heuristic argument is correct, and the representation (2)

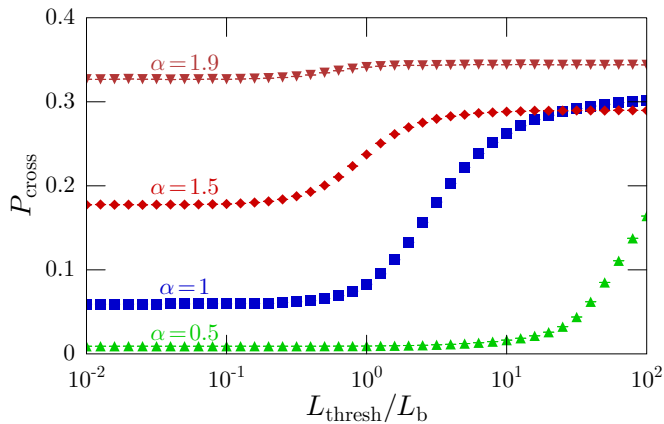


FIG. 6. Simulated probability for Lévy bridges generated via Eq. (2) to cross a boundary at $d = \sigma T^{1/\alpha}$, as the rejection threshold L_{thresh} varies.

is valid—any ballistic “stretch” does not affect the Gaussian statistics in the continuum limit. It fails, however, for $\alpha < 2$: if $x(T)$ corresponds to a sufficiently large final displacement, then the stretch is excessive, and the resulting “bridges” produce erroneous results in simulations. (Reference [40] noted this inequivalence between stretched and conditioned bridges [54].)

Since we have a large-step criterion, it is possible to deal with excessive stretches. The fix is to define a threshold L_{thresh} , and an unconditioned Lévy sample path is only stretched as in Eq. (2) if its final point $L = x(T)$ is within L_{thresh} of the bridge’s arrival point. Otherwise, it is rejected and other paths attempted until a bridge is successfully generated. The α -dependent bifurcation length L_b from Fig. 4 marks a scale L_{thresh} below which the stretching algorithm should yield an accurate set of Lévy bridges. A test of this algorithm, computing the probability P_{cross} for Lévy bridges (with $L = 0$) to cross a boundary at $d = \sigma T^{1/\alpha}$ before time T , illustrates this transition (Fig. 6) [55]. In particular, the simulated P_{cross} rapidly becomes accurate when L_{thresh} decreases below L_b (the bridge construction is exact in the limit $L_{\text{thresh}} \rightarrow 0$). As a practical bridge-generation method, this is much more efficient than using $\sigma \Delta t^{1/\alpha}$ (the smallest natural length scale) for L_{thresh} .

A particularly interesting feature in Fig. 6 is that $P_{\text{cross}} = 0.9\%$ is so small for the case $\alpha = 0.5$. (By contrast, $P_{\text{cross}} = 31.5\%$ in the unconditioned case.) The surprise here is that the smallest- α case has the strongest tendency towards large jumps—intuitively, the best “mobility”—and yet has the smallest boundary-crossing probability. However, conditioning on $L = 0$ also conditions away the tendency to have extreme jumps (and thus to easily cross the boundary), precisely because an extreme jump is suppressed by the requirement of a compensating (and correspondingly rare) jump to return to the final target state.

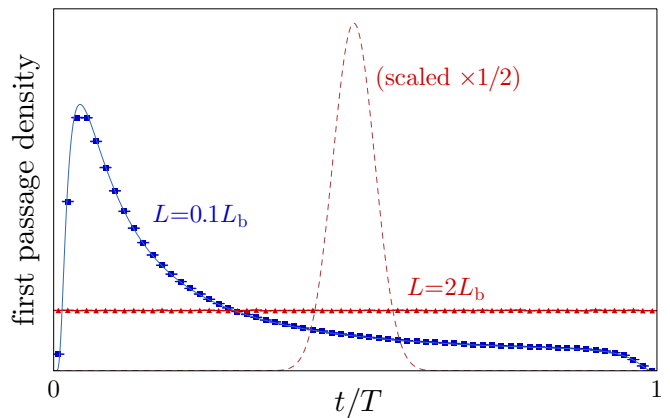


FIG. 7. Simulated conditioned first passage time distributions for $\alpha = 1.99999$ and $d = L/2$ are shown for $L = 0.1L_b$ (blue/squares) and $L = 2L_b$ (red/triangles). Exact densities for $\alpha = 2$ [25] for the same L values are shown for comparison in each case (blue, solid and red, dashed, respectively).

B. Conditioned first passage

First-passage times, defined here as the first time a process $x(t)$ exceeds a boundary d , are of broad importance [56]. They are especially interesting for Lévy processes due to the universal Sparre Andersen scaling [21, 22, 57], where the tail of the first-passage-time distribution is α -independent. However, as we have seen, conditioned Lévy bridges have a particularly sensitive transition as $\alpha \rightarrow 2$, a pattern that continues for first-passage times.

An intuitive picture of the conditioned first-passage time follows from the qualitative appearance of the sample paths for $L = 1.5L_b$ in Fig. 5. A dominant jump is consistently present among the paths, but not at any particular time. This can be regarded as an outcome of recursively sampling the midpoint density (1). For $L \gg L_b$, a large step likely persists under sampling iterations, but due to the symmetry of the midstep distribution, the large step is equally likely to be associated with any time subinterval. Since the first-passage time is likely due to the dominant jump, the first-passage time should be uniformly distributed. Figure 7 confirms this intuition with simulations of the first passage density [58]. For $L = 2L_b$ the first passage density is indeed uniform. A small change from $\alpha = 1.99999$ to the Gaussian case yields a remarkably different distribution: approximately Gaussian, centered at $t \approx T/2$. The Gaussian result follows intuitively from Eq. (2), since the most likely bridges in this regime are concentrated around the ballistic path to the endpoint.

For a smaller overall displacement ($L = 0.1L_b$), the first-passage-time densities in the $\alpha = 1.99999$ and Gaussian cases match closely. This is consistent with the observation that for $L \ll L_b$, the conditioned Lévy bridges are qualitatively similar to Brownian bridges. Nevertheless, the rare but important extreme jumps generate remarkably non-Gaussian behavior, even close to the Gaus-

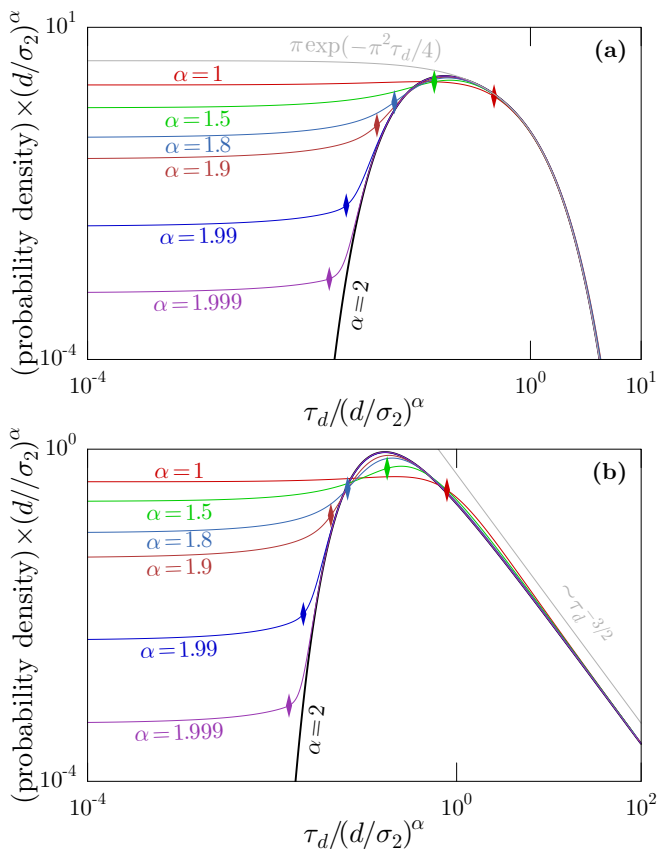


FIG. 8. (a) Simulated first-escape-time distributions from $(-d, d)$ for various Lévy processes starting at $x = 0$, showing long-time behavior that matches Gaussian ($\alpha = 2$) behavior, but diverging short-time behavior. (b) Simulated first-passage distributions [i.e., first escape from $(-\infty, d)$] show similar behavior. The bifurcation time T_b is marked by a diamond symbol in each case. The width-scaling parameter σ is chosen for each α to obtain matching asymptotic behavior, as discussed in the main text.

sian limit.

C. Unconditioned first escape

The major theme of this paper has been the conditioned evolution of stochastic processes. However, the reasoning we have used thus far is useful in studying unconditioned evolution as well. As a common example, consider the first-escape time of a stable Lévy process starting at $x = 0$ from the interval $(-d, d)$, $\tau_d := \inf\{t : |x(t)| \geq d\}$. The simulated probability densities for the escape time for various values of α are shown in Fig. 8(a). The striking feature of this set of distributions is the universal, α -independent asymptotic behavior at long times. Each of the probability distributions splits away from the Gaussian ($\alpha = 2$) distribution at a point that is different for each value of α .

To understand the behavior here, first note that the

portion of the escape-time distribution to the left of any particular time τ acts as a conditioned density, because it refers only to the subset of trajectories that has escaped by time τ . This implicit conditioned behavior allows us to apply our results for conditioned processes to this simple escape-time problem. The bifurcation length L_b is of particular utility here. Recall that a long jump must have occurred in an escape by time τ if $d > L_b = \tilde{L}_b \sigma \tau^{1/\alpha}$, where \tilde{L}_b is the value of the bifurcation length L_b given by setting $\sigma = T = 1$. Rearranging this expression, we can define the bifurcation timescale T_b such that an escape by time τ must have involved a long jump if $\tau < T_b := (d/\sigma)^\alpha / \tilde{L}_b^\alpha$. This bifurcation time is marked as a diamond on each distribution in Fig. 8(a), and it evidently marks the timescale where the escape-time distribution for each stable Lévy case splits away from the Gaussian limit. For large escape times $\tau_d \gg T_b$, an extreme jump is unlikely, and any Lévy process behaves basically as a Gaussian random walk. On the other hand, for small escape times $\tau_d \ll T_b$, a single large jump is the most likely scenario. In this case the reasoning of Sec. IV B applies, and the dominant jump is equally likely to occur at any time below a fixed $\tau \ll T_b$. In the escape-time distributions, this behavior appears as an asymptotically constant behavior of the distribution as $\tau_d \rightarrow 0$ (where in the Gaussian case, the probability density vanishes here). This constant value of the density at small escape times decreases with increasing α , as expected because the probability of an extreme jump also decreases (owing to the less-fat tails). The universality of the long-time asymptotic tail here is thus another example of the intuition we mentioned above that heavy-tailed processes resemble Gaussian processes between occurrences of rare, extreme events.

Figure 8(b) shows the analogous behavior for (unconditioned) first-passage densities $\tau_d := \inf\{t : x(t) \geq d\}$, corresponding to escape from the interval $(-\infty, d)$. The division between Gaussian-like and extreme-event behavior is also apparent here—the main difference is the form of the asymptotic tail, which has the characteristic Sparre Andersen scaling of $\sim \tau_d^{-3/2}$.

At this point some brief comments clarifying the simulated distributions in Fig. 8 are in order. The distributions were computed by numerical integration of the fractional diffusion equation [59]. It is most sensible to compare distributions with the same long-time asymptotic behavior, accomplished by an appropriate choice for the α -dependent width-scale parameter σ_α . For the first-escape problem, the asymptotic tail is of the form $e^{-\sigma_\alpha^\alpha \lambda_1^{(\alpha)} t/d^\alpha}$ [60], where $\lambda_1^{(\alpha)}$ is the smallest eigenvalue of the fractional Laplace operator $(-\nabla^2)^{\alpha/2}$ on the bounded domain $[-1, 1]$ (e.g., $\lambda_1^{(2)} = \pi^2/4$ in the Gaussian limit). The asymptotics thus match across α via the choice $\sigma_\alpha^\alpha / \sigma_2^2 = \pi^2/4 d^{2-\alpha} \lambda_1^{(\alpha)}$, using the Gaussian scale parameter σ_2 as a reference. The asymptotic tail in the first-passage problem has the form $(d/\sigma)^\alpha / \alpha \sqrt{\pi} \Gamma(\alpha/2) \tau^{3/2}$ [24]. These asymptotics match for the choice $\sigma_\alpha^\alpha / \sigma_2^2 = 1/d^{2-\alpha} \Gamma^2(1 + \alpha/2)$.

The bifurcation time (and thus length) mark a boundary between Gaussian and extreme-event behavior in a conceptually simple setting of the escape problem, which is directly amenable to experimental observation. For example, we have already mentioned that laser-cooled atoms are an important prototype system for studying Lévy-type dynamics [13–20] (including the big-jump principle [43]). A setup appropriate for the study of escape times is that of a single laser-cooled atom monitored by a fluorescence-detection system [14, 61]. An aperture for the fluorescence photodetector defines the region from which the atom is to escape; the time that it takes to observe a sharp drop in the atomic fluorescence after the release of the atom (from its initially prepared position) is a measure of the escape time. A more detailed discussion of the Lévy behavior of laser-cooled atoms as well as typical parameters for an experimental realization are included in the Supplemental Material [62]. Of course, beyond laser-cooled atoms, this first-escape behavior should be observable in essentially any stochastic physical system that is accurately modeled by stable Lévy processes.

V. SUMMARY

We have discussed the conditioned evolution of α -stable Lévy processes as a prototype for extreme events. The knowledge of a particular final state turns out to retrodict whether an extreme event occurred along the way. This conclusion follows from an analysis of the conditioned densities, which change form as the final displacement passes a threshold, the bifurcation length. The analysis here has applications to the construction of Lévy bridges, the qualitative understanding of conditioned first-passage dynamics, and the understanding of unconditioned first-escape problems. We have also pointed out how the manifestation of the bifurcation length in the first-escape problem can be studied experimentally with laser-cooled atoms.

ACKNOWLEDGMENTS

We gratefully acknowledge helpful discussions with Steven van Enk. This work was supported by the NSF (PHY-1505118) and NVIDIA Corporation.

-
- [1] S. Albeverio, V. Jentsch, and H. Kantz, eds., *Extreme Events in Nature and Society* (Springer, Berlin, 2006).
- [2] J. Beirlant, Y. Goegebeur, J. Teugels, J. Segers, D. D. Waal, and C. Ferro, *Statistics of Extremes: Theory and Applications* (Wiley, Chichester, 2004).
- [3] R. Cont and P. Tankov, *Financial Modeling with Jump Processes* (Chapman & Hall, Boca Raton, 2004).
- [4] C. Gardiner, *Stochastic Methods: A Handbook for the Natural and Social Sciences*, 4th ed. (Springer, Berlin, 2009).
- [5] K. Jacobs, *Stochastic Processes for Physicists: Understanding Noisy Systems* (Cambridge University Press, Cambridge, 2010).
- [6] M. F. Shlesinger, G. M. Zaslavsky, and U. Frisch, eds., *Lévy Flights and Related Topics in Physics: Proceedings of the International Workshop Held at Nice, France, 27–30 June 1994* (Springer, Berlin, 1995).
- [7] V. V. Uchaikin and V. M. Zolotarev, *Chance and Stability. Stable Distributions and their Applications* (VSP, Utrecht, 1999).
- [8] G. M. Viswanathan, V. Afanasyev, S. V. Buldyrev, E. J. Murphy, P. A. Prince, and H. E. Stanley, *Nature* **381**, 413 (1996).
- [9] T. H. Solomon, E. R. Weeks, and H. L. Swinney, *Phys. Rev. Lett.* **71**, 3975 (1993).
- [10] M. F. Shlesinger, G. M. Zaslavsky, and J. Klafter, *Nature* **363**, 31 (1993).
- [11] R. Metzler, T. Koren, B. van den Broek, G. J. L. Wuite, and M. A. Lomholt, *J. Phys. A Math. Gen.* **42**, 434005 (2009).
- [12] V. V. Palyulin, A. V. Chechkin, and R. Metzler, *Proc. Natl. Acad. Sci. U.S.A.* **111**, 2931 (2014).
- [13] S. Marksteiner, K. Ellinger, and P. Zoller, *Phys. Rev. A* **53**, 3409 (1996).
- [14] H. Katori, S. Schlipf, and H. Walther, *Phys. Rev. Lett.* **79**, 2221 (1997).
- [15] F. Bardou, J.-P. Bouchaud, A. Aspect, and C. Cohen-Tannoudji, *Lévy Statistics and Laser Cooling: How Rare Events Bring Atoms to Rest* (Cambridge University Press, Cambridge, 2002).
- [16] Y. Sagi, M. Brook, I. Almog, and N. Davidson, *Phys. Rev. Lett.* **108**, 093002 (2012).
- [17] D. A. Kessler and E. Barkai, *Phys. Rev. Lett.* **108**, 230602 (2012).
- [18] E. Barkai, E. Aghion, and D. A. Kessler, *Phys. Rev. X* **4**, 021036 (2014).
- [19] G. Afek, J. Coslovsky, A. Courvoisier, O. Livneh, and N. Davidson, *Phys. Rev. Lett.* **119**, 060602 (2017).
- [20] E. Aghion, D. A. Kessler, and E. Barkai, *Phys. Rev. Lett.* **118**, 260601 (2017).
- [21] G. Zumofen and J. Klafter, *Phys. Rev. E* **51**, 2805 (1995).
- [22] A. V. Chechkin, R. Metzler, V. Y. Gonchar, J. Klafter, and L. V. Tanatarov, *J. Phys. A Math. Gen.* **36**, L537 (2003).
- [23] B. Dybiec, E. Gudowska-Nowak, and P. Hänggi, *Phys. Rev. E* **73**, 046104 (2006).
- [24] T. Koren, M. A. Lomholt, A. V. Chechkin, J. Klafter, and R. Metzler, *Phys. Rev. Lett.* **99**, 160602 (2007).
- [25] A. N. Borodin and P. Salminen, *Handbook of Brownian Motion: Facts and Formulae*, 2nd ed. (Birkhäuser, Basel, 2002).
- [26] D. C. Brody, L. P. Hughston, and A. Macrina, in *Advances in Mathematical Finance*, edited by M. C. Fu, R. A. Jarrow, J.-Y. J. Yen, and R. J. Elliott (Birkhäuser, Boston, 2007) p. 231.
- [27] B. Moskowitz and R. E. Caffisch, *Math. Comput. Model.* **23**, 37 (1996).
- [28] C. Chiarella, *Ecology* **88**, 2354 (2007).

- [29] H. Gies, K. Langfeld, and L. Moyaerts, *J. High Energy Phys.*, **018** (2003).
- [30] J. B. Mackrory, T. Bhattacharya, and D. A. Steck, *Phys. Rev. A* **94**, 042508 (2016).
- [31] P. Levitz, D. S. Grebenkov, M. Zinsmeister, K. M. Kolwankar, and B. Sapoval, *Phys. Rev. Lett.* **96**, 180601 (2006).
- [32] D. S. Dean, A. Iorio, E. Marinari, and G. Oshanin, *Phys. Rev. E* **94**, 032131 (2016).
- [33] F. Mori, S. N. Majumdar, and G. Schehr, *Phys. Rev. Lett.* **123**, 200201 (2019).
- [34] A. Perret, A. Comtet, S. N. Majumdar, and G. Schehr, *Phys. Rev. Lett.* **111**, 240601 (2013).
- [35] M. Delorme and K. J. Wiese, *Phys. Rev. E* **94**, 052105 (2016).
- [36] M. Dlask, J. Kukal, M. Poplová, P. Sovka, and M. Cifra, *PLoS ONE* **14**, 1 (2019).
- [37] E. Hoyle, L. P. Hughston, and A. Macrina, *Stoch. Process. Their Appl.* **121**, 856 (2011).
- [38] E. Hoyle, L. P. Hughston, and A. Macrina, in *Advances in Mathematics of Finance, Banach Center Publications, vol. 104*, edited by A. Palczewski and Lukasz Stettner (Polish Academy of Sciences, Warsaw, 2015) pp. 95–120.
- [39] P. J. Fitzsimmons and R. K. Gettoor, *Stoch. Process. Their Appl.* **58**, 73 (1995).
- [40] F. B. Knight, in *Hommage à P. A. Meyer et J. Neveu*, Astérisque No. 236 (Société mathématique de France, 1996) p. 171.
- [41] L. Chaumont, D. G. Hobson, and M. Yor, *Séminaire de probabilités de Strasbourg* **35**, 334 (2001).
- [42] N. N. Taleb, *The Black Swan: The Impact of the Highly Improbable*, 2nd ed. (Random House, New York, 2010).
- [43] A. Vezzani, E. Barkai, and R. Burioni, *Phys. Rev. E* **100**, 012108 (2019).
- [44] R. Burioni and A. Vezzani, *J. Stat. Mech.: Theory Exp.* **2020**, 034005 (2020).
- [45] S. N. Majumdar, in *Exact Methods in Low-dimensional Statistical Physics and Quantum Computing (Lecture Notes of the Les Houches Summer School: Volume 89, July 2008)*, edited by J. Jacobsen, S. Ouvry, V. Pasquier, D. Serban, and L. Cugliandolo (Oxford University Press, New York, 2010) pp. 407–429.
- [46] J. Szavits-Nossan, M. R. Evans, and S. N. Majumdar, *Phys. Rev. Lett.* **112**, 020602 (2014).
- [47] J. Szavits-Nossan, M. R. Evans, and S. N. Majumdar, *J. Phys. A: Math. Theor.* **47**, 455004 (2014).
- [48] G. Gradenigo and S. N. Majumdar, *J. Stat. Mech.: Theory Exp.* **2019**, 053206 (2019).
- [49] The term “bifurcation” here refers to the behavior of the maxima of the probability densities, behavior analogous to the bifurcation of the stable points in a quartic potential. This bifurcation terminology has been applied to a probability density in the same sense by C. Chiarella, *Eur. J. Political Econ.* **7**, 65 (1991) in an economic stochastic-process model; by contrast, the bifurcation we discuss arises naturally from the conditioned stable Lévy densities themselves.
- [50] A. V. Nagaev and S. M. Shkol’nik, *Theory Probab. Its Appl.* **33**, 139 (1989).
- [51] M. L. Stein, *Interpolation of Spatial Data: Some Theory for Kriging* (Springer, New York, 1999).
- [52] C. Schluter and M. Trede, *J. Empir. Finance* **15**, 700 (2008).
- [53] I. Karatzas and S. E. Shreve, *Brownian Motion and Stochastic Calculus*, 2nd ed. (Springer, Berlin, 1991).
- [54] Another inequivalent representation was studied by A. Janicki and A. Weron, *Simulation and Chaotic Behavior of α -Stable Stochastic Processes* (Marcel Dekker, New York, 1994).
- [55] Simulations used $\Delta t = 10^{-5}T$, averaging over 10^7 paths.
- [56] S. Redner, *A Guide to First Passage Processes* (Cambridge University Press, Cambridge, 2001).
- [57] J. Klafter and I. M. Sokolov, *First Steps in Random Walks: From Tools to Applications* (Oxford University Press, Oxford, 2011).
- [58] Simulations averaged 10^7 paths, with $\Delta t = 2^{-14}T$.
- [59] S. Watanabe, *J. Math. Soc. Japan* **14**, 170 (1962).
- [60] B. Dybiec, E. Gudowska-Nowak, E. Barkai, and A. A. Dubkov, *Phys. Rev. E* **95**, 052102 (2017).
- [61] W. Alt, *Optik* **3**, 142 (2002).
- [62] See Supplemental Material for a discussion of the observability of the effects described in this paper in experiments with laser-cooled atoms, which includes Refs. [63–66].
- [63] J. Dalibard and C. Cohen-Tannoudji, *J. Opt. Soc. Am. B* **6**, 2023 (1989).
- [64] S. Jonsella, C. Dion, M. Nylén, S. J. H. Petra, P. Sjölund, and A. Kastberg, *Eur. Phys. J. D* **39**, 67 (2006).
- [65] F. Svensson, S. Jonsell, and C. M. Dion, *Eur. Phys. J. D* **48**, 235 (2008).
- [66] E. Lutz, *Phys. Rev. A* **67**, 051402(R) (2003).

**Supplementary material for the manuscript “The anatomy of an
extreme event: What can we infer about the history of a
heavy-tailed random walk?”**

Wesley W. Erickson and Daniel A. Steck

*Oregon Center for Optical, Molecular,
and Quantum Science and Department of Physics,
1274 University of Oregon, Eugene, OR 97403-1274*

In this document we provide an overview of Lévy-type behavior of laser-cooled atoms, along with simulations of first-escape times. We also provide sample parameters for a possible experimental study of the bifurcation length in this context.

I. SISYPHUS COOLING AND LÉVY DYNAMICS

Atoms cooled by laser light have been an important physical realization of Lévy-type behavior, in both theory and experiment [1–8]. The Sisyphus mechanism [9] is a particular process by which atoms with degenerate (fine or hyperfine) energy-level structure can be laser-cooled below the limits of the Doppler-cooling mechanism. Sisyphus cooling in one dimension provides a particularly clean and well studied realization of Lévy behavior [1, 2, 4–8].

The physical setup for Sisyphus cooling involves an atom moving in a light field produced by a pair of counterpropagating laser beams with orthogonal linear polarizations. The equations of motion describing the momentum and position of an atom moving in such a laser field may be written [1, 6]

$$\begin{aligned} dp &= -\frac{p}{1+p^2} dt + \sqrt{2D} dW \\ dx &= p dt, \end{aligned} \tag{1}$$

where $dW(t)$ is the differential element of a Wiener process $W(t)$, and these equations of motion are expressed in dimensionless units defined by

$$\tilde{p} := \frac{p}{p_c}, \quad \tilde{x} := \frac{m\bar{\alpha}}{p_c} x, \quad \tilde{D} := \frac{D_1}{\bar{\alpha}p_c^2}, \quad \tilde{t} := \bar{\alpha}t, \tag{2}$$

after dropping the twiddles. The constants describing the underlying atom–laser interaction are given by

$$\frac{p_c}{\hbar k} = \frac{2\hbar\Gamma s_0}{9\ 4E_r}, \quad \bar{\alpha} = 6\frac{|\Delta|}{\Gamma}, \quad \frac{D_1}{(\hbar k)^2\omega_r} = \frac{41\ \Gamma s_0}{90\ \omega_r} \tag{3}$$

where the recoil energy is given in terms of the atomic mass m and the optical wave number k by

$$E_r = \hbar\omega_r = \frac{\hbar^2 k^2}{2m}, \tag{4}$$

and the atomic saturation parameter is given by

$$s_0 = \frac{I/I_{\text{sat}}}{1 + 4\Delta^2/\Gamma^2} \tag{5}$$

in terms of the (angular) detuning Δ of the laser frequency from the atomic resonance, the excited-state decay rate Γ , the maximum laser intensity I , and the atomic saturation intensity I_{sat} . The above equations are specific to the structure of a $J = 1/2 \rightarrow J' = 3/2$ transition, and the saturation intensity refers to the $m = 1/2 \rightarrow m' = 3/2$ sub-transition. We will discuss the 780-nm transition in ^{87}Rb , which has a more complicated level structure. Modeling such a more complicated is limited to numerical treatment [10, 11], but the above equations nevertheless produce good qualitative agreement with experiments [4], and so we employ them here. For ^{87}Rb , then, $I_{\text{sat}} = 1.67 \text{ mW/cm}^2$.

In terms of the scaled diffusion parameter D , the molasses behavior maps onto Lévy behavior in the range $1/5 < D < 1$ via

$$\alpha = \frac{1 + D}{3D}, \quad (6)$$

where α is the Lévy parameter falling in the range $2/3 < \alpha < 2$. The anomalous diffusion coefficient is

$$K_\alpha = \frac{1}{\mathcal{Z}} \frac{\pi(3\alpha - 1)^{\alpha-1}}{\sin(\pi\alpha/2)3^{2\alpha-1}|\Gamma(\alpha)|^2}, \quad \mathcal{Z} = \sqrt{\pi} \frac{\Gamma[(1 - D)/2D]}{\Gamma(1/2D)}, \quad (7)$$

defined such that the width of the Lévy distribution scales with t as form $(K_\alpha t)^{1/\alpha}$, so that the width parameter in the main article is given by $\sigma = (K_\alpha)^{1/\alpha}$.

II. ESCAPE-TIME SIMULATIONS

Due to the nonzero time taken to make large, Lévy-type jumps, there is a cutoff where Lévy-type behavior breaks down at a length scale [6]

$$x \sim \sqrt{D} t^{3/2}. \quad (8)$$

In a first-escape-time experiment with two barriers at distance d on either side of the atomic starting position, this implies a characteristic “cutoff” time scale

$$t_c \sim \left(\frac{d}{\sqrt{D}} \right)^{2/3}, \quad (9)$$

below which we do not expect the first-passage/escape time to be described well by Lévy behavior. This time scale is sensibly specified in units where the barrier distance and Lévy

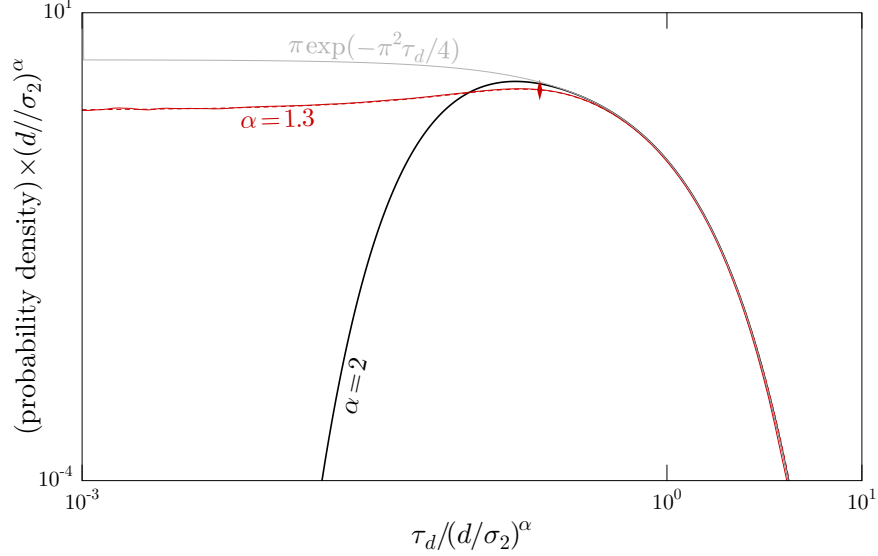


FIG. 1. (Color online.) Simulated probability density for the first-escape time τ_d (the smallest time t for which $|x(t)| \geq d$) for Sisyphus-cooled atoms (solid red curve) and Lévy processes (dashed red curve), both with Lévy index $\alpha = 1.3$. The Gaussian case ($\alpha = 2$, heavy solid black curve) is also shown for reference. The bifurcation time T_b is marked with a diamond. No rescaling of the distributions was performed here to align the asymptotic behaviors for different α , in contrast with the main article.

diffusion constant K_α have been scaled out of the dynamical evolution; switching to this scaled time, we can define this cutoff time scale as

$$t_c := \frac{d^{2/3-\alpha} K_\alpha}{D^{1/3}}. \quad (10)$$

This time scale is a parameter in the atomic simulations that must be specified independently of α , with smaller values yielding higher-fidelity Lévy dynamics.

The simulations here were performed using a second-order method for additive stochastic differential equations, with a fixed time step $\Delta t = 0.1$. The simulations all used $t_c = 10^{-4}$ (note that this cutoff time in “simulation units” was chosen to satisfy $t_c(d^\alpha/K_\alpha) \gg \Delta t$), which is used in Eq. (10) to determine the appropriate half-width d of the escape region. The maximum time of the simulations were $T = 10 d^\alpha/K_\alpha$. Every trajectory started with $x = 0$ at $t = 0$, and the initial momentum was chosen randomly for each trajectory from the steady-state (Tsallis) momentum distribution [12]. The first-escape time τ_d was then taken to be the first time for each trajectory where $|x(t)| \geq d$. The simulated first-escape-time distributions each employed ensembles of 10^7 trajectories.

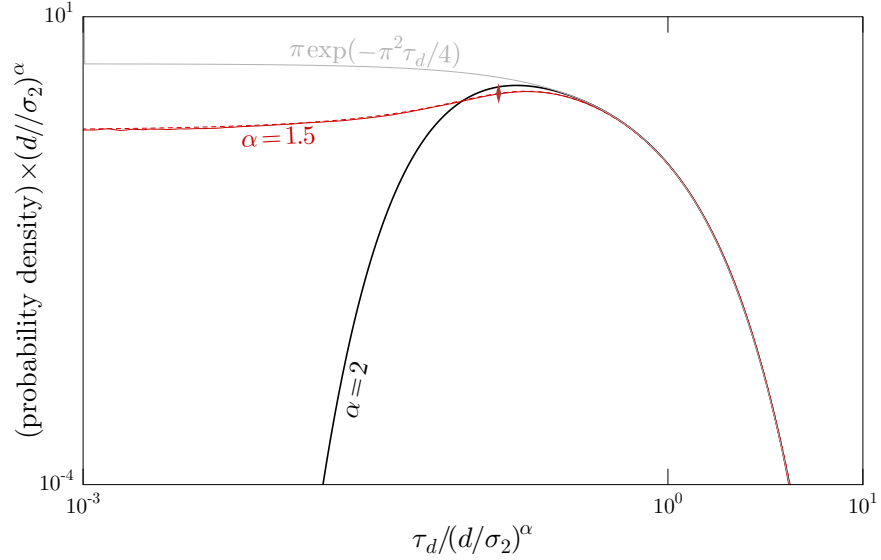


FIG. 2. (Color online.) Simulated probability density for the first-escape time τ_d as in Fig. 1, but with $\alpha = 1.5$.

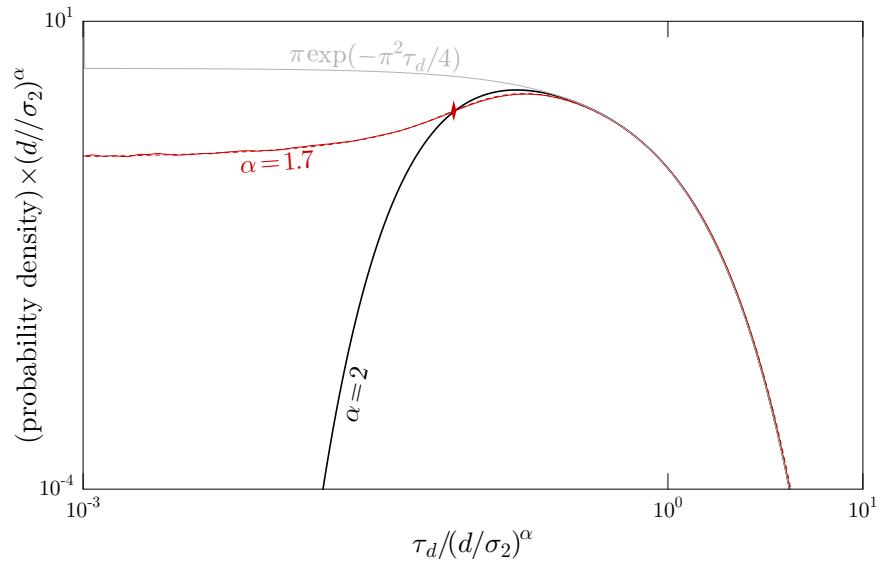


FIG. 3. (Color online.) Simulated probability density for the first-escape time τ_d as in Fig. 1, but with $\alpha = 1.7$.

Simulated escape-time distributions are shown for the cases $\alpha = 1.3$ (Fig. 1), $\alpha = 1.5$ (Fig. 2), $\alpha = 1.7$ (Fig. 3), $\alpha = 1.8$ (Fig. 4), and $\alpha = 1.9$ (Fig. 5), along with the computed distributions of escape times for the corresponding Lévy-process trajectories. In the first three cases, the laser-cooled-atom simulations closely match the Lévy-process simulations. In the last two cases, however, while there is qualitative agreement between the atomic and

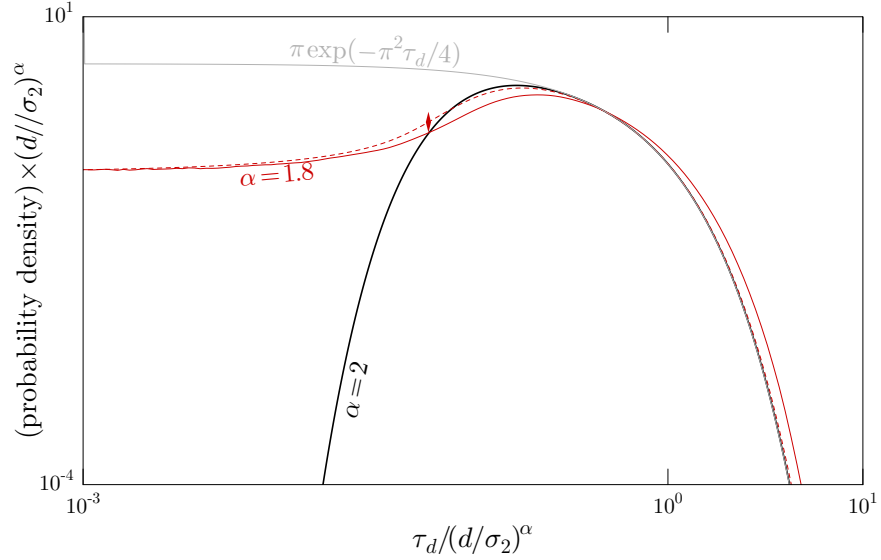


FIG. 4. (Color online.) Simulated probability density for the first-escape time τ_d as in Fig. 1, but with $\alpha = 1.8$.

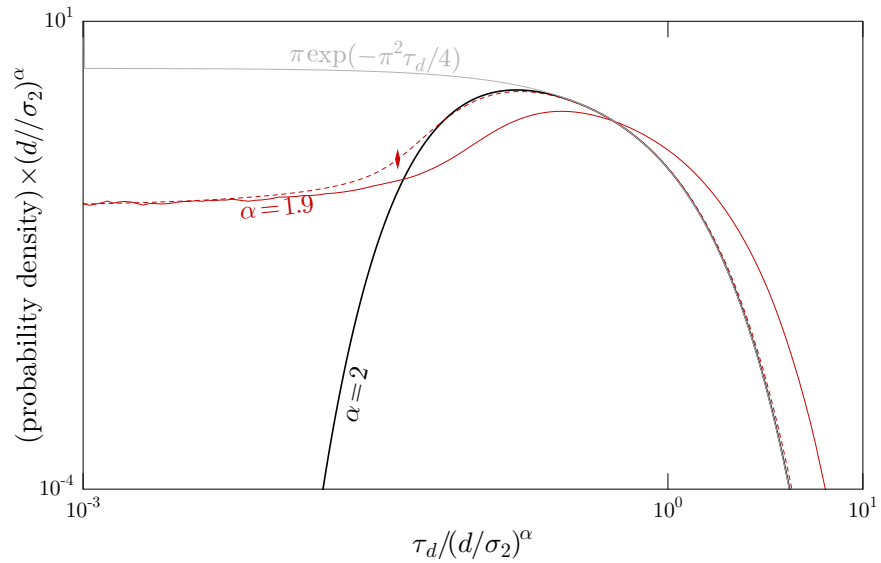


FIG. 5. (Color online.) Simulated probability density for the first-escape time τ_d as in Fig. 1, but with $\alpha = 1.9$.

Lévy simulations, the distributions do not quantitatively match. For $\alpha = 1.8$, the peak of the atomic distribution is shifted by a factor of about 1.16 compared to the Lévy distribution, and for $\alpha = 1.9$, the observed shift is by a factor of about 1.60. The cause of this shift is a slow settling in to the asymptotic Lévy behavior in the near-Gaussian (α close to 2) regime. That is, the atomic and Lévy first-escape-time distributions will agree better over longer

α	T_b	I/I_{sat}	d	shift factor
1.3	397 ms	1.8	2.0 mm	1.0
1.5	209 ms	2.1	128 μm	1.0
1.7	105 ms	2.5	28 μm	1.0
1.8	71 ms	2.7	19 μm	1.16
1.9	45 ms	2.9	17 μm	1.60

TABLE I. Sample set of physical parameters for the laser-cooled-atom simulations.

time scales, accomplished by choosing smaller value of t_c . Choices of t_c much below 10^{-4} are difficult to simulate due to the long computation times involved, though they should be accessible experimentally, as we discuss below. In any case, the conclusion here is that laser-cooled atoms can be used in first-escape experiments to study the bifurcation time (which is marked in each of the plots), although depending on the chosen parameters, a correction factor may be necessary to account for deviations between atomic and idealized Lévy dynamics.

III. PHYSICAL PARAMETERS

Finally, we discuss the conversion of the above parameters into physical units. Once α and t_c have been specified, only one more parameter, the laser detuning Δ from atomic resonance, needs to be specified to fix the parameters for the atom–laser interaction. For simplicity, we choose a constant $\Delta = -10\Gamma$ for all the parameter sets here; this is a typical value in laser-cooling setups, and it is similar to the value used in ^{87}Rb -based experiments [4]. The physical parameters for this choice of laser detuning and t_c for various values of the Lévy index α are shown in Table I. Recall that the experiment involves releasing an atom at the center of the escape region and into the optical lattice that effects Sisyphus cooling. The measurement is to record the time it takes to leave the escape region of half-width d . The escape region is set by an optical aperture for the photodetector that monitors the presence of the atom in the escape region. The intensities (given in units of the saturation intensity) are typical of laser-cooling experiments, and easily achievable. The bifurcation time scales determine the order of magnitude of the times that the experiment must manage; this time scale ranges from tens to hundreds of ms, which are experimentally reasonable (previous

experiments studied atomic expansions in the range of tens of ms [4]). The range of width parameters for the escape region runs from tens of μm to a few mm. This parameter should be large compared to the atomic resonance wavelength (780 nm for ^{87}Rb) in order to sharply resolve the edges of the regime. Note that for $\alpha > 2/3$, T_b and d are related to an inverse power of t_c , so it is straightforward to increase or decrease the physical length and time scales. The main cost of increasing t_c is a larger possible discrepancy with Lévy behavior, which can be explicitly accounted for. There is no real downside to decreasing t_c , though simulations may become computationally expensive as noted above. Finally, it is important to choose physical parameters such that Doppler cooling—ignored in Eqs. (1)—does not significantly inhibit Lévy-type behavior [1]. Here, this is guaranteed by choosing a relatively large detuning compared to Γ , as has been verified experimentally [4].

-
- [1] S. Marksteiner, K. Ellinger, and P. Zoller, *Phys. Rev. A* **53**, 3409 (1996).
 - [2] H. Katori, S. Schlipf, and H. Walther, *Phys. Rev. Lett.* **79**, 2221 (1997).
 - [3] F. Bardou, J.-P. Bouchaud, A. Aspect, and C. Cohen-Tannoudji, *Lévy Statistics and Laser Cooling: How Rare Events Bring Atoms to Rest* (Cambridge University Press, Cambridge, 2002).
 - [4] Y. Sagi, M. Brook, I. Almog, and N. Davidson, *Phys. Rev. Lett.* **108**, 093002 (2012).
 - [5] D. A. Kessler and E. Barkai, *Phys. Rev. Lett.* **108**, 230602 (2012).
 - [6] E. Barkai, E. Aghion, and D. A. Kessler, *Phys. Rev. X* **4**, 021036 (2014).
 - [7] G. Afek, J. Coslovsky, A. Courvoisier, O. Livneh, and N. Davidson, *Phys. Rev. Lett.* **119**, 060602 (2017).
 - [8] E. Aghion, D. A. Kessler, and E. Barkai, *Phys. Rev. Lett.* **118**, 260601 (2017).
 - [9] J. Dalibard and C. Cohen-Tannoudji, *J. Opt. Soc. Am. B* **6**, 2023 (1989).
 - [10] S. Jonsella, C. Dion, M. Nylén, S. J. H. Petra, P. Sjölund, and A. Kastberg, *Eur. Phys. J. D* **39**, 67 (2006).
 - [11] F. Svensson, S. Jonsell, and C. M. Dion, *Eur. Phys. J. D* **48**, 235 (2008).
 - [12] E. Lutz, *Phys. Rev. A* **67**, 051402(R) (2003).